Electron Transport Properties in BN Molecular Junction from First-Principles Calculations

Y. Zhao a,b , Y. Mu^c, C. Hu^d and Y. Cheng b,*

Received: 23.04.2025 & Accepted: 22.08.2025

Doi: 10.12693/APhysPolA.148.114

*e-mail: ycheng@scu.edu.cn

Density functional theory and non-equilibrium Green's function method are used to study the contact geometry and electron transport properties of BN molecules coupled with Au (100) electrodes. We calculated the conductance of four different coupling morphologies to simulate the stretching and breaking process of the Au–BN–Au molecular junction. The calculated results yield the equilibrium distances of the four configurations as $d_z=12.631,\ 9.844,\ 10.024,\ 6.424$ Å; equilibrium conductances are 0.228 G_0 , 0.975 G_0 , 0.813 G_0 , 5.201 G_0 , indicating that the BN nanojunction has good electron transport properties. A key finding is that within the voltage range from -1.6 to 1.6 V, the current-voltage of nearly all junctions shows a linear relationship, indicating that the BN molecular junction has metal-like properties under low bias voltage. The asymmetry of the I-V curves directly reflects the asymmetry in molecular structure and coupling morphology. These results confirm that the conductance of BN nanojunctions is strongly influenced by the coupling morphology, electrode distance, and external bias voltage of the electrode-connected BN molecules, with the metal-like transport behavior and morphological asymmetry under bias emerging as critical characteristics.

topics: BN molecular junction, electron transport, equilibrium conductance, nonequilibrium Green's functions

1. Introduction

Since the invention of integrated circuits, the size of various electronic devices has continued to shrink. In 1959, Richard Feynman first proposed a physically feasible approach to further miniaturization of devices, i.e., the use of single molecules, or even atoms, to assemble functional electronic components. This bottom-up strategy for constructing electronic devices has opened up a new field focused on building nanostructures, nanodevices, nanocircuits, and nanointegrated systems using single molecules. At the mesoscopic scale, techniques such as the mechanically controllable break junction (MCBJ) method [1], electromigration [2], and scanning tunneling microscopy (STM) [3] for studying the electron transport characteristics of the basic unit of the molecule, thus designing and preparing electronic devices with various functions such as information storage, transmission, conversion, detection, and processing, have opened up a new way for the sustainable development of electronics. Since then, domestic and foreign scholars have conducted in-depth studies on the transport characteristics of many molecular devices and discovered various interesting phenomena, such as negative differential resistance [4–8], conductance quantization [9, 10], rectification function [11], etc. Therefore, molecular electronics [12, 13] has become a hot topic in the fields of physics and materials science.

Using molecules or atomic clusters directly to construct electronic devices has many advantages due to their small size, wide range of materials, low fabrication costs, and low energy consumption. Intermolecular interactions can be used to achieve self-assembly of different structures. Various physical properties of molecules can also be manipulated at will to achieve different functions of the device. Among many molecules, the simplest diatomic ones are directly connected to Au, Ag, Pt, Pd, and other electrodes to form molecular junctions, and their electron transport properties are studied to obtain valuable results [1, 14–28]. For example, Smit et al. [20] found that H₂ molecules can form stable Pt–H₂ molecular junctions with Pt electrodes

^aLuoyang Institute of Science and Technology, Luoyang 471023, China

^bCollege of Physics, Sichuan University, Chengdu 610064, China

^cSchool of Physics and Electronic Engineering, Sichuan Normal University, Chengdu 610066, China

^dCollege of Physics and Electronic Engineering, Chongqing Normal University, Chongqing 400047, China

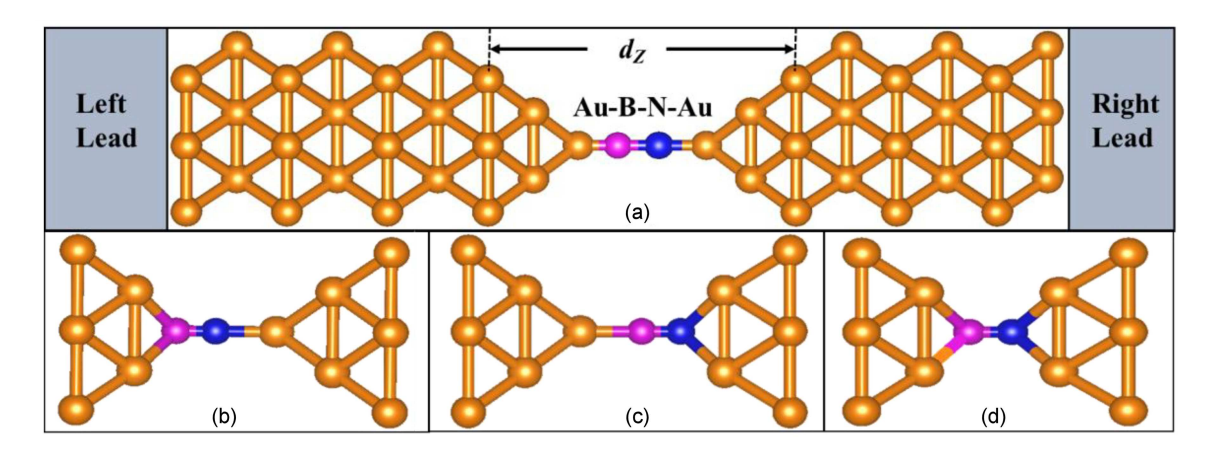


Fig. 1. BN nanojunction models with different coupling configurations: (a) top-top configuration with the B, N bonds axis separately parallel to the transport direction (top-top parallel), (b) hollow-top configuration, (c) top-hollow configuration, and (d) hollow-hollow configuration.

in a hydrogen-rich environment. At this time, the conductance and current of the Pt-H₂ molecular junction have changed significantly. Similarly, Thijssen et al. [21] found that Ag electrodes and O_2 molecules can form Ag-O₂, and the conductance of Ag-O₂ molecular junctions is significantly different from that of pure Ag molecular junctions. Later, Strange et al. [22] found that Pt electrodes can form Pt-CO-Pt molecular junctions with CO molecules. They explained the transport mechanism of molecular devices based on the electronic structure of the molecule. Yu et al. [16] calculated the influence of different coupling morphologies on the electron transport properties of the S₂ cluster, and the results showed that the I-V curves of the four configurations of S₂ molecular junctions showed linear characteristics. Liu [23-26] studied the electron transport properties of GaAs and small silicon clusters and found that they all have electron transport behavior similar to metals.

As an important III-V inorganic non-metallic material, BN exhibits a series of excellent physical and chemical properties, and it has important prospects for future applications in molecular devices. The structures and properties of BN clusters have also attracted the interest of many researchers. At present, one-dimensional (1D) boron nitride nanowires (BNNWs) [29, 30] have been successfully experimentally synthesized, and the BN chain has been successfully fabricated by irradiating h-BN sheets with electron beams [31, 32]. Theoretically, Zhang et al. [33] constructed a series of periodic three-dimensional (3D) BN molecular structures termed T-B_xN_x (x = 4n - 1, n = 1, 2, 3, ...),and their density functional theory (DFT) calculations showed that these molecules have strong metal properties. Based on the interest in these $T-B_xN_x$ molecular units with novel properties, Wang et al. [34, 35] constructed 3D BN molecular junctions and investigated their electronic transport characteristics. Zeng et al. [36] used non-equilibrium

Green's function to study the electron transport properties of a boron nitride chain between twodimensional (2D) metal boron-benzene electrodes. They found that when the BN chain is coupled with the 2D boron-benzene electrode, it exhibits metallic characteristics and negative differential resistance behavior. Although the BN nanostructures and their quantum transport properties have been studied, the electrical transport properties of nanojunctions containing a single BN molecule have not been revealed, including the coupling morphology between the molecule and the electrodes, the electrode distance, and the applied bias, which have not been discussed in detail yet. Therefore, theoretical understanding of the electrical transport characteristics of the simplest BN clusters is crucial for their application in electronic devices.

In this work, we focus on the influence of molecular contact geometry on the conductivity and I-V characteristics of BN molecules sandwiched between two Au electrodes. We simulated the stretching process of the Au–BN–Au junctions in four different anchoring geometries and obtained the I-V characteristics of the nanojunctions at the equilibrium position.

2. Computational details

In this work, we use the SIESTA [37] program, based on DFT [38], to optimize the structures of the molecular junctions and conduct theoretical calculations of the electronic structure. The TranSIESTA module is used to study the properties of electronic transport. This method uses non-equilibrium Green's function (NEGF) [39] to perform first-principles quantum modeling of molecules. Our theoretical model consists of a single BN molecule coupled with two semi-infinite Au (100) metal electrodes. The dual probe system can be divided into

three regions: the left electrode, the right electrode, and the central scattering area. The central scattering area contains BN molecules and seven layers of Au atoms on the left and six layers on the right to shield against the interference of molecules on the electrodes [40].

For the Au–BN–Au molecular junctions, we have investigated four possible coupling structures, as shown in the respective panels in Fig. 1:

- (a) a BN molecule connected to the atoms at the top of the pyramid electrodes, forming a top—top structure;
- (b) a structure with the Au atom removed at the tip of the electrode pyramid on the left and BN connected to the hollow position on the left and the top position on the right to form a hollow-top configuration;
- (c) a structure with the Au atom removed at the tip of the pyramid on the right side electrode and BN connected to the top position on the left and the hollow position on the right to form a top-hollow configuration;
- (d) a structure with the Au atom removed at the tips of the electrode pyramids on both sides, and BN is connected to the hollow positions on both sides to form a hollow-hollow configuration.

Electron transmission in all four configurations occurs along the z-axis. Two semi-infinite electrodes are considered to be perfect crystals, and their chemical potential is very close to that of a perfect bulk electrode. For the central scattering region, the electron potential is calculated self-consistently under each applied bias [41–43]. The value of the current flowing through the molecule can be obtained from the Landauer–Buttiker [44] formula

$$I(V) = \frac{2e}{h} \int dE \ T(E, V) \Big[f(E - \mu_L) - f(E - \mu_R) \Big],$$
(1)

where f is the Fermi–Dirac distribution function and $\mu_{L/R}$ is the chemical potential of the left/right electrode. The integration interval is $[\mu_L, \mu_R]$, which means $[E_{\rm F} - \frac{eV}{2}, E_{\rm F} + \frac{eV}{2}]$, where $E_{\rm F}$ is the Fermi level. The transmission T(E,V) is related to the electron incident energy E and the applied bias voltage V. When the system is in equilibrium and the external bias voltage V=0 V, the equilibrium conductance G of the system can be obtained by multiplying the quantum conductance $(G_0=2e^2/h)$ by the transmission $T(E=E_{\rm F},V=0$ V), namely

$$G = \frac{2e^2}{h} T(E = E_F, V = 0).$$
 (2)

In theoretical calculations, we use the local density approximation (LDA) method, and the exchange—correlation function adopts the parameterized functional in the Perdew—Zunger form [45]. The Troullier—Martins pseudopotential [46] and the Kleinman—Bylander approximation [47] with

non-local mode conservation are used to describe the inner electrons, and the linear combination of a finite range of numerical atomic orbitals is used to describe the valence electrons. The valence electron orbitals of Au atoms use the single ζ polarization (SZP) basis set, and both the B and N atoms use the double ζ polarization (DZP) basis set. The Au (100) surface contains 3×3 atoms; the self-consistent calculation cutoff energy is 300 Ry, and the energy convergence standard is 10^{-4} .

3. Results and discussion

3.1. Simulation of the stretching process

When the BN molecule is connected to two half-infinite Au electrodes, changes in atomic interactions at the coupling interface alter the junction structure, so the geometry of the junction should be optimized before calculating the electron transport properties. For the relaxation of the BN molecule and pyramid-shaped Au atoms while keeping the remaining electrode layers fixed, we define the distance between the two pyramid bases, d_z (as shown in Fig. 1), and the binding energy

$$\Delta E = E(Au-BN-Au) - E(Au \text{ electrodes})$$

$$-E(BN molecule).$$
 (3)

The calculated $\Delta E - d_z$ relationships for each configuration are shown in Fig. 2. The relationships ΔE versus d_z curves of all configurations show a parabolic shape, which means that they all correspond to the most stable equilibrium structures. Figure 2 shows that the stable equilibrium positions of the four configurations in panels (a)–(d) are, respectively, $d_z = 12.631, 9.844, 10.024, 6.424 \text{ Å}$; the binding energies ΔE of the corresponding junctions are -8.311, -9.508, -8.816, -6.856 eV, suggesting that the stability order of the systems is (b) > (c) >(a) > (d). This stability trend exhibits distinct characteristics compared to other III-V molecular junctions reported in the literature. For instance, Zhang et al. [48] investigated GaN molecular junctions and found that their most stable configuration typically occurs at a larger inter-electrode distance $(\approx 11.5 \text{ Å for GaN in a top-top configuration})$, with a binding energy of ≈ -7.2 eV, which is weaker than the energy of -8.311 eV observed in our BN top-top configuration (a). Similarly, studies on InN molecular junctions [16] revealed a stability order dominated by hollow-hollow configurations with binding energies around -5.9 eV, which is significantly lower than our BN hollow-hollow configuration (d) at -6.856 eV. This indicates that BN — despite its smaller molecular size compared to GaN or InN forms stronger bonds with Au electrodes, likely due to the higher electronegativity difference between B and N (3.04 for N, 2.04 for B) enhancing charge transfer at the interface [49].

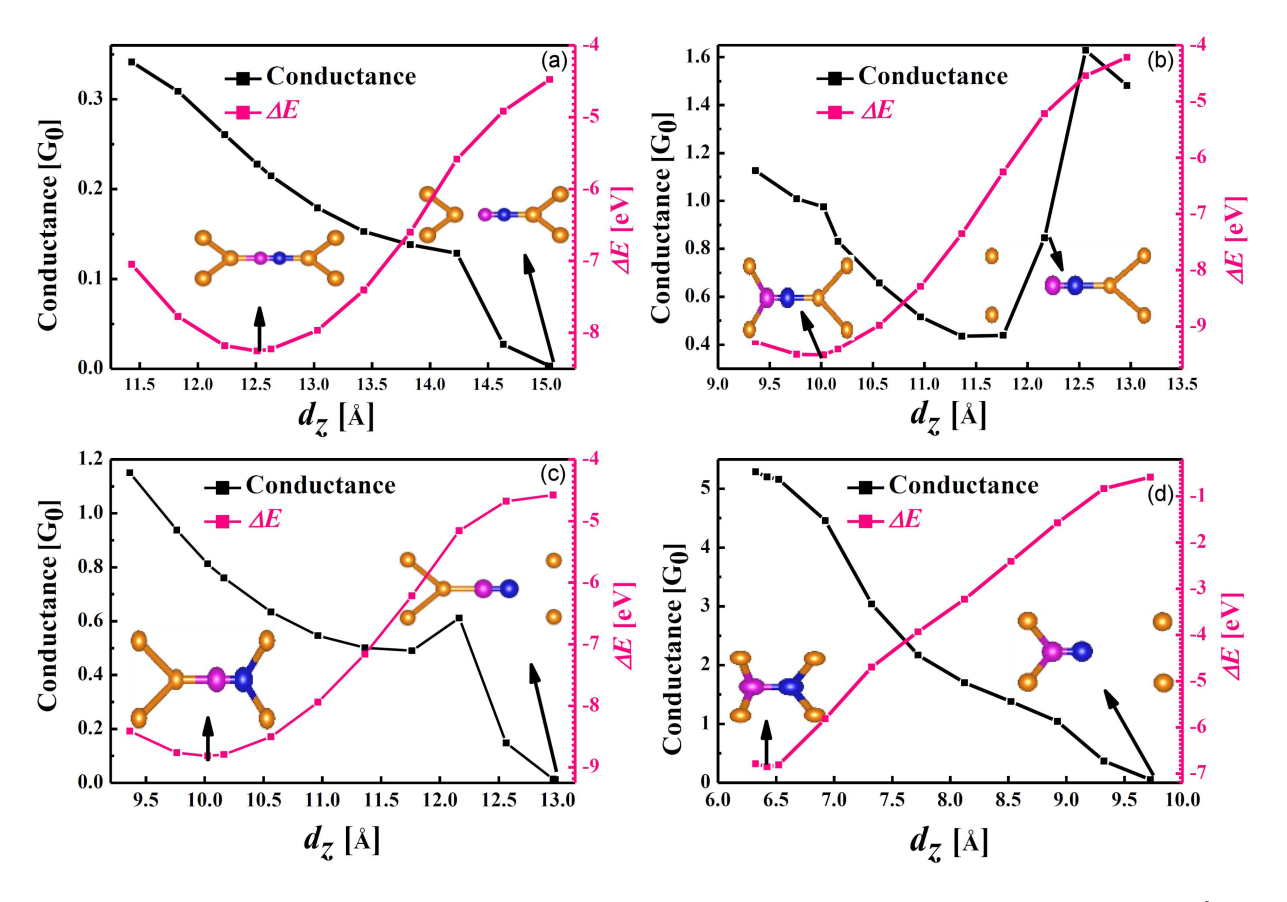


Fig. 2. The relationship between binding energy ΔE [eV] and conductance G [G_0] with distance d_z [Å]: (a) top-top configuration, (b) hollow-top configuration, (c) top-hollow configuration, and (d) hollow-hollow configuration. Here, d_z represents the distance between the two Au electrodes along the transport direction, ΔE quantifies the stability of the junction (a more negative value indicates stronger binding and higher structural stability), and G characterizes the efficiency of electron transport ($G_0 = 2e^2/h$).

At the same time, we calculated the bond lengths of Au-B, Au-N, and B-N when each configuration is in a stable equilibrium position. For configuration (a), the Au-B bond length is 2.003 Å and the Au-N bond length is 1.932 Å. The bond length of B-N is 1.267 Å, which is shorter than the experimentally observed B-N single bond length of 1.31 Å [31] and the theoretically calculated 1.300 Å [50–52]. This difference may be due to the reduced coordination number in the BN structure of the diatomic molecule and the complex hybridization between the molecule and the electrodes [53]. For configurations (b) and (c), B-N bond lengths are 1.298 and 1.317 Å, respectively, which are close to the experimental and theoretical calculations. In configuration (d), the B-N bond is 1.393 Å. The B and N atoms in this configuration have the largest nearestneighbor coordination number, and the interaction between the B and N atoms and the four Au atoms on its side is highly intense. Notably, the variation in B-N bond lengths across configurations contrasts with trends in GaN molecular junctions. Zhang et al. [48] reported Ga-N bond lengths in GaN junctions ranging from 1.96 to 2.05 Å, with minimal dependence on electrode coupling geometry — likely

due to Ga's larger atomic radius limiting structural flexibility. In contrast, our BN system shows a 10% variation in B–N bond length (1.267–1.393 Å) across configurations, reflecting stronger sensitivity to interfacial geometry. This flexibility could be advantageous for tuning electronic properties, a feature less pronounced in heavier III–V counterparts like InN [25].

We also calculated the equilibrium conductance at different distances d_z during the stretching process, as shown in Fig. 2. For configuration (a), as the structure stretches, the conductivity of the configuration decreases from 0.341 G_0 at $d_z = 11.431$ Å to 0.027 G_0 at $d_z = 14.631$ Å, which is the breaking point of the Au-B bond. In configuration (b), the conductance decreases from 1.126 G_0 at $d_z = 9.364 \text{ Å to } 0.085 \text{ } G_0 \text{ at } d_z = 12.164 \text{ Å, which}$ is the breaking point of the Au-B bond. For configuration (c), the conductance decreases from 1.150 G_0 at $d_z = 9.364 \text{ Å to } 0.612 \text{ } G_0 \text{ at } d_z = 12.164 \text{ Å}, \text{ and}$ then suddenly drops to 0.014 G_0 at $d_z = 12.964$ Å, at which point the Au-N bond breaks. Finally, for configuration (d), as the distance increases, the conductance gradually decreases from 5.288 G_0 at $d_z = 6.324 \text{ Å to } 0.053 \text{ } G_0 \text{ at } d_z = 9.724 \text{ Å, which is}$

the breaking point of the Au-N bond. The conductance values observed in BN junctions are significantly higher than those reported for other III-V systems. For example, GaN molecular junctions exhibit maximum conductances of $\simeq 0.5 G_0$ [48], while InP junctions [52] rarely exceed 0.3 G_0 . The peak conductance of $5.288~G_0$ in our BN hollow-hollow configuration (d) is particularly striking, surpassing even the high conductance of $2.1 G_0$ reported for InAs junctions [53]. This suggests that BN's diatomic structure facilitates more efficient electron transport pathways compared to the larger, more complex III-V molecules, where electron scattering at bulk-like molecular orbitals reduces conductance. Additionally, the conductance sensitivity to stretching (e.g., a 20-fold drop in configuration (d)) is more pronounced than in GaN junctions [48], where conductance decreases by only 3-5 times over similar distance ranges, highlighting BN's potential as a highly responsive nanoscale sensor. Throughout the whole process, it is not difficult to see that, except for some unstable points, the conductivity decreases with the extension of the connection in the four configurations. This indicates that the conductance of the junction is very sensitive to the contact distance between the two electrodes and the change of the coupling morphology. In other words, it reveals the sensitivity of conductance to local atomic rearrangements in the contact area [54]. This behavior is characteristic of the coherent transport mechanism and a direct manifestation of the wave nature of charge carriers. When the four configurations (Fig. 1a-d) are in a stable equilibrium structure, their equilibrium conductances are 2.228 G_0 , $0.975 G_0$, $0.813 G_0$, and $5.201 G_0$, respectively.

Additionally, we focus on the spatial electron density difference when the structures break for the four configurations, as shown in Fig. 3. The electron density difference is defined as

$$\rho'(r) = \rho(r) - \rho_{\text{atoms}}(r), \tag{4}$$

where $\rho(r)$ is the self-consistently calculated electron density of the junctions after structural breakage, and $\rho_{\text{atoms}}(r)$ is that of free atoms placed at the same positions. Chemical bonds with electron density differences can be identified by the positions of electron accumulation or dispersion and atomic coordinates. Figure 3 shows the uneven distribution of the electron cloud in the fractured structure. The charge is more distributed between the B-N atoms, indicating that the B and N atoms form a strong chemical bond. The minimum distribution of electron differential density corresponds in phase to the fractured chemical bond. The charge accumulation patterns at breakage differ markedly from those in GaN junctions. In GaN systems [48], charge depletion dominates at the metal-molecule interface during fracture, reflecting ionic bond character. In contrast, our BN junctions show persistent charge accumulation between B and N even at breaking points, suggesting covalent bond retention

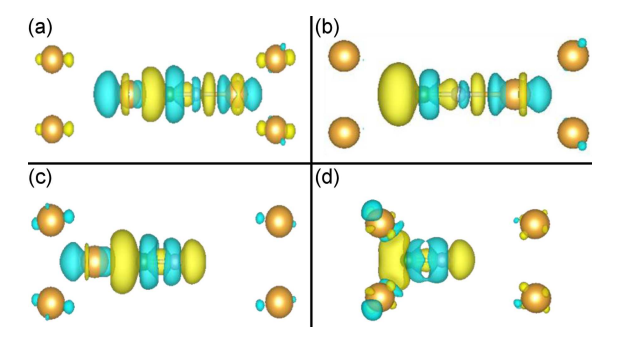


Fig. 3. Spatial electron density difference around the Fermi level of the BN molecule at the corresponding break point: (a) top-top configuration $(d_z=14.631~\text{Å})$, (b) hollow-top configuration $(d_z=12.164~\text{Å})$, (c) top-hollow configuration $(d_z=12.964~\text{Å})$, (d) hollow-hollow configuration $(d_z=9.724~\text{Å})$. The value of the isosurface is 0.03. The yellow (blue) electron cloud indicates an increase in charge density amount (reduction).

— a feature also observed in *ab initio* studies of BN nanotubes [51]. This covalent stability likely contributes to BN's higher conductance retention during stretching compared to ionic III–V compounds.

3.2. Transmission spectrum and projected density of states

In order to better understand the transport characteristics and transport channels of the Au-BN-Au junctions, we can analyze the transmission spectrum T(E, V=0) (see Fig. 4) and the projected density of states (PDOS) (see Fig. 5) of the BN molecular junctions. As can be seen in Fig. 4a, the transmission spectra of the four configurations are relatively flat near the Fermi surface; this indicates that the interaction between the BN molecule and the electrodes is relatively strong, and the overlap of the electron cloud makes the molecular energy level broaden, and the density of states becomes a continuous distribution, so there are no obvious peaks. This flat transmission spectrum near the Fermi level contrasts with the sharp resonant peaks observed in GaN [48] and InN [16] junctions, which arise from discrete molecular orbitals weakly coupled to electrodes. The absence of peaks in BN suggests stronger molecule—electrode hybridization, consistent with its higher conductance. A similar flat transmission profile was reported for InAs junctions [53], but with lower overall transmission coefficients ($\simeq 1.2$ in InAs vs 5.2 in BN). This indicates that BN achieves both strong coupling and high electron transparency. The strength of the interaction can also be reflected by the binding energy of the central scattering region. From the results in Fig. 2, it can be seen that configuration (b) has the largest binding energy, and configuration (d)

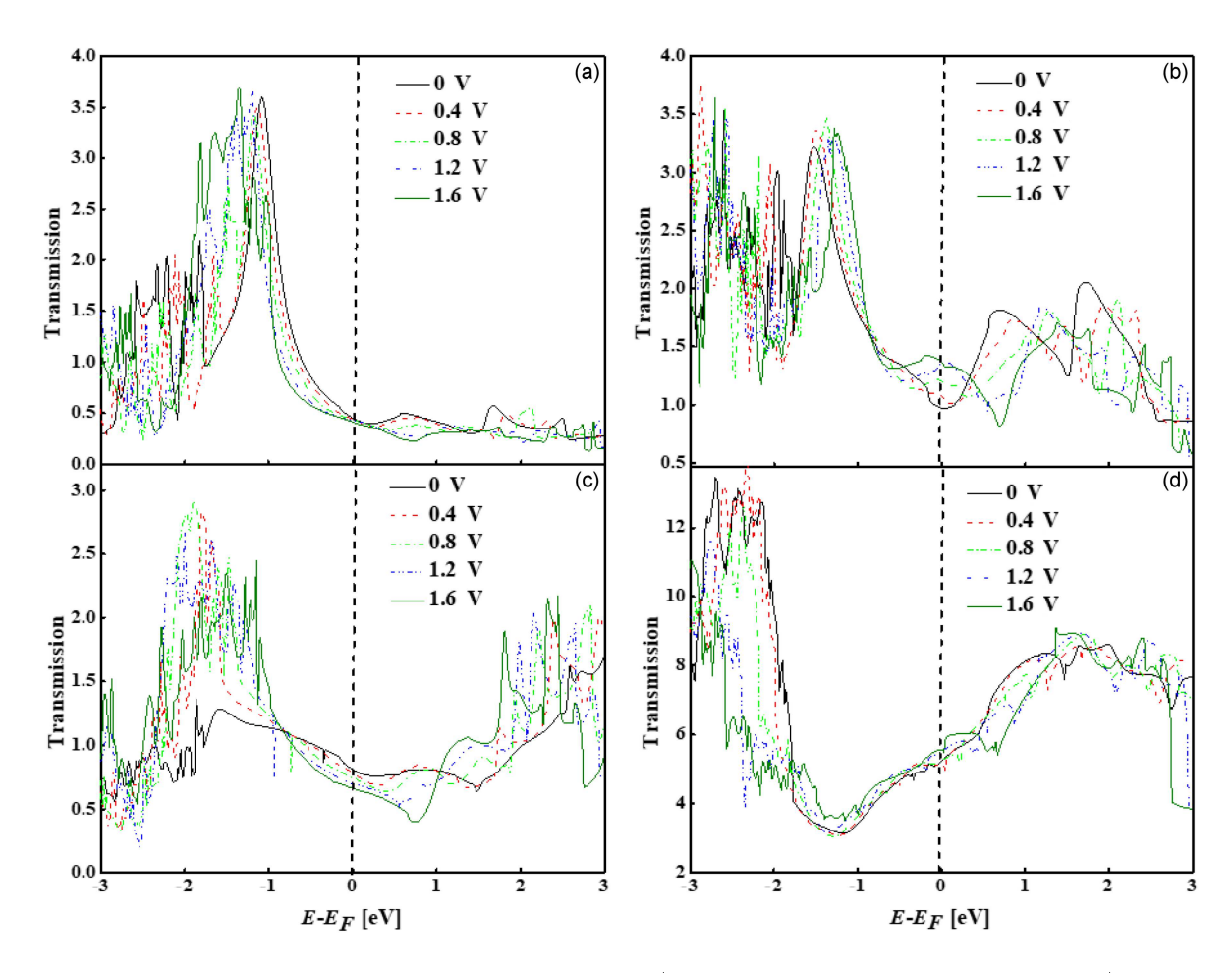


Fig. 4. Transmission coefficients as a function of energy (relative to the Fermi level, $E-E_{\rm F}$, in eV) for BN nanojunctions at their optimal stable positions (d_z where the binding energy is most negative, indicating highest structural stability) under different external biases (0 V, ± 0.4 V, ± 0.8 V, ± 1.2 V, ± 1.6 V). The transmission coefficient quantifies the probability of electron transport through the nanojunction at a given energy. Panels (a)–(d) correspond to top–top, hollow–top, top–hollow, and hollow–hollow configurations, respectively.

has the smallest binding energy, which corresponds to their transmission spectrum. The transmission coefficients of the four stable structures (Fig. 1a–d) at the Fermi surface $E_{\rm F}$ are: 2.228, 0.975, 0.813, and 5.201, respectively.

To better understand the transport channel, we further analyze the projected density of states (PDOS) of the molecular junctions. For configuration (a), the transport channel is mainly formed by the p_x and p_y orbital electrons of the B and N atoms. For configuration (b), due to the coupling of the B atom and the hollow on the Au (100) surface, the contribution of the $p_x + p_y$ orbital electrons to the transport channel is much smaller than that of the N atom. For (c), the N atom is coupled with the hollow, so its p_x+p_y orbital electrons contribute less to the transport channel. For (d), due to its equilibrium distance $d_z = 6.424$ Å, which is the shortest among the four configurations, the electronic coupling is the strongest, which leads to a significant broadening of the resonance, and the transmittance becomes flat near the Fermi level. The transmission channels are mainly formed by electrons in the p_x+p_y orbital of B and N atoms, and their p_z orbital contribution is almost negligible. The orbital-dependent transport in BN differs from GaN, where p_z orbitals dominate conduction due to Ga's larger atomic size, favoring axial hybridization [48]. BN's reliance on p_x/p_y orbitals aligns with its planar symmetry, a feature shared with InP junctions [52], but with higher orbital overlap efficiency. This orbital selectivity could enable BN-based junctions to exhibit direction-dependent conductivity, a property less pronounced in bulkier III–V molecules.

3.3. *I–V* characteristic curves and rectification ratio

It is well known that changes in transport characteristics are related to the details of the frontier orbitals of the BN molecule and the applied voltage. The applied bias will change the Hamiltonian operator of the molecular junction and affect its conductance. Figure 6 illustrates the current—voltage

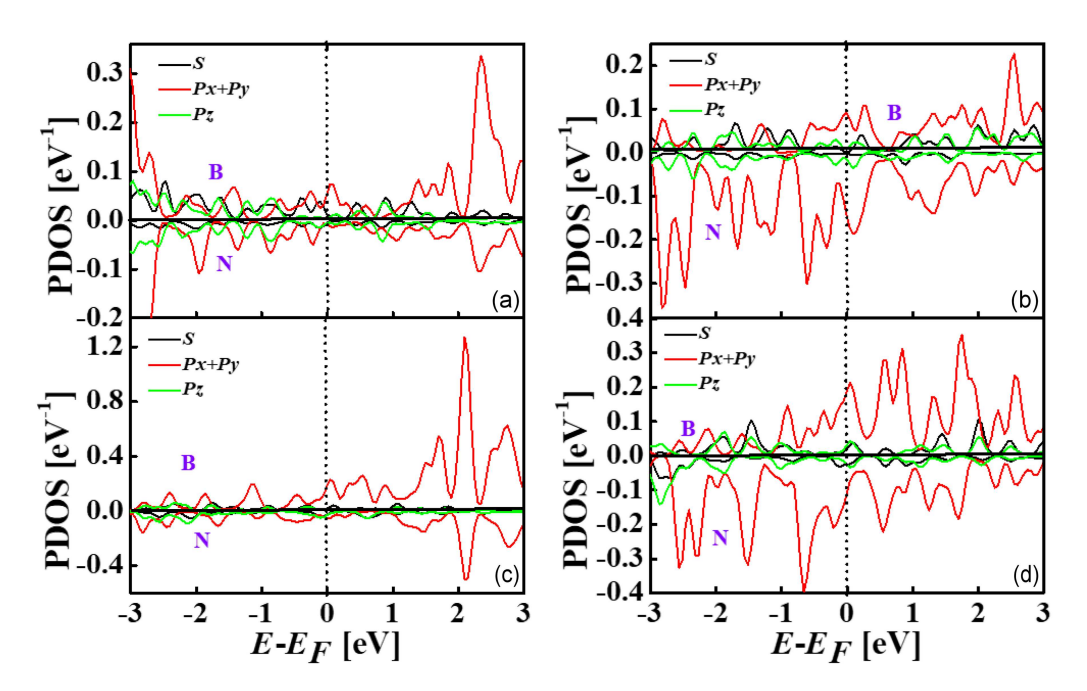


Fig. 5. Projected density of states (PDOS) of the BN molecule in BN nanojunctions at their optimal stable positions. PDOS describes the distribution of electronic states (per unit energy) localized on the BN molecule, with the energy axis referenced to the Fermi level $(E_{\rm F})$. Panels (a)-(d) correspond to top-top, hollow-top, top-hollow, and hollow-hollow configurations, respectively.

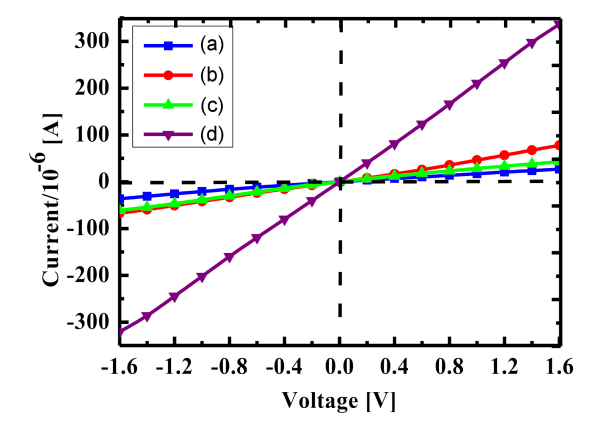


Fig. 6. Current–voltage (I-V) characteristics of BN nanojunctions at their optimal stable positions, showing the relationship between the current (I) flowing through the nanojunction and the applied bias voltage (V) across the two Au electrodes. Panels (a)–(d) correspond to top–top, hollow–top, top–hollow, and hollow–hollow configurations, respectively. The current is a direct measure of the nanojunction's conductivity under external bias; note that higher current indicates more efficient electron transport.

relationship of the four configurations in the bias voltage from -1.6 to 1.6 V. It can be seen in Fig. 6 that the I-V curves of the four configurations are all linear and exhibit metal-like characteristics within the considered voltage range. This linearity is a key novelty compared to other III-V systems. GaN [48]

and InN [16] junctions show strong nonlinearity with voltage thresholds ($\simeq 0.5$ V) due to their semiconductor-like band gaps, while BN's metallic behavior (linear I-V up to 1.6 V) resembles that of metallic atomic junctions [54]. This suggests that BN could bridge the gap between molecular electronics (typically semiconducting) and atomic-scale metallic contacts, offering unique integration potential. Under the same bias voltage, the order of the magnitude of the current is (d) > (c) > (b) > (a). Considering the symmetry of the device, symmetrical I-V characteristics are expected under symmetrical coupling [23, 55]. However, on the contrary, the I-V curves we get for each configuration are asymmetric. In Fig. 6, for configurations (a) and (c), the current at V < 0 is greater than that at V > 0; for configurations (b) and (d), the opposite is true. This asymmetry may arise from the inherent polarity of the BN molecule and asymmetric coupling with the electrodes, as has been confirmed in other theories [25, 56, 57] and experiments [56]. The rectification ratios in BN (peaking at $\simeq 2.5$ in configuration (d)) are moderate compared to GaN's rectification ratios of $\simeq 5$ [48], but are achieved without the band gap dependence that limits GaN's operating range. Importantly, BN's rectification persists at higher biases (1.6 V) than GaN (< 1.0 V), making it more suitable for high-voltage nanodevices. The directionality of rectification (e.g., positive bias preference in (b)/(d)) also differs from GaN's universal negative bias preference [48], enabling complementary circuit design when combined with other III-V junctions.

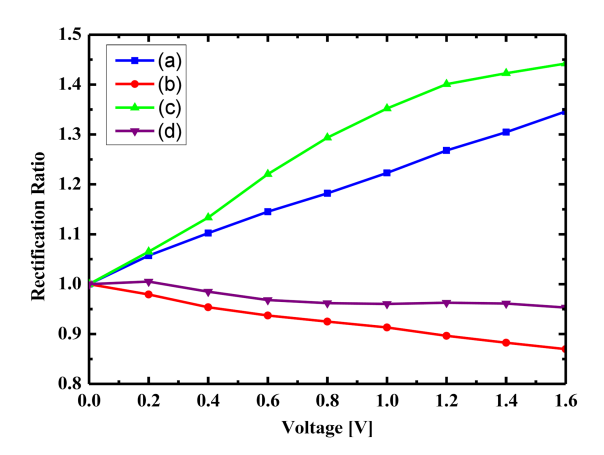


Fig. 7. Rectification ratios of BN nanojunctions at their optimal stable positions as a function of applied bias voltage. The rectification ratio is a key metric for evaluating the rectification effect (unidirectional conduction) of the nanojunction. The designations (a)-(d) in the legend correspond to the top-top, hollow-top, top-hollow, and hollow-hollow configurations, respectively.

Another example is the study by Zhang et al. [48] on the electrical transport properties of GaN molecular junctions. Their research shows that the I-V curves of GaN molecular junctions are nonlinear and asymmetric, indicating semiconductor-like properties of these junctions. The current asymmetry can be quantified by the reverse rectification ratio of the molecular junction changing with the bias voltage, which is defined as [58]

$$R(V) = \left| \frac{I(-V)}{I(+V)} \right|. \tag{5}$$

Figure 7 shows the change curves of the rectification ratio of the molecular junctions with the bias voltage. It can be seen in the figure that the reverse rectification ratios of configurations (a) and (c) are greater than 1, which indicates that the current under negative bias is greater than that under positive bias. As the bias voltage increases, the rectification effect is significantly enhanced. The configurations (b) and (d) are the opposite.

The above analysis shows that under a certain bias, the current flowing through the molecular junction is related to the structure and properties of the molecule itself and the geometric contact configuration of the interface. The transport characteristics of the molecular junction can be tuned through appropriate molecular design to fabricate molecular devices with specific functions.

4. Conclusions

In summary, we have applied density functional theory and non-equilibrium Green's function methods to systematically study the electronic transport

characteristics of BN molecules sandwiched between two semi-infinite Au (100) electrodes in four different coupling morphologies. We have simulated the stretching and breaking process of Au-BN-Au molecular junctions and calculated the binding energies and conductances at different tensile distances. The calculated stable equilibrium positions of the four configurations (Fig. 1a-d) are $d_z = 12.631$, 9.844, 10.024, 6.424 Å, respectively; the corresponding binding energies are -8.311, -9.508, -8.816, -6.856 eV, suggesting that the order of stability of the molecular junctions is (b) > (c) > (a) > (d). The equilibrium conductances are $0.228 \ G_0, \ 0.975 \ G_0, \ 0.813 \ G_0, \ 5.201 \ G_0, \ respec$ tively. It can be concluded that the conductance of the molecular junction is very sensitive to the local atomic rearrangement at the contact interface, and the BN molecular junctions have good conductivity. The B-N bond lengths are 1.267, 1.298, 1.317, 1.393 Å, respectively. In comparison, configuration (d) has the largest equilibrium conductance and current; the wide and strong transmission peak near the Fermi level indicates strong interaction between the BN molecule and the Au electrodes in the hollow-hollow configuration. We have also calculated the relationship between the current and the applied bias voltage in four different configurations (Fig. 1a-d). It has been found that the current in configurations (a) and (c) under the negative bias voltage is greater than the current under the positive bias voltage, while the opposite is true for configurations (b) and (d). This behavior shows that the BN junctions have metal-like characteristics.

Acknowledgments

The authors are grateful to the Head of the Department of Physics for providing the departmental facilities and to Professor Xiangrong Chen, School of Physics, Sichuan University, for his guidance.

References

- M.A. Reed, C. Zhou, C.J. Muller, T.P. Burgin, J.M. Tour, *Science* 278, 252 (1997).
- [2] H. Park, J. Park, A.K.L. Lim, E.H. Anderson, A.P. Alivisatos, P.L. Mceuen, *Nature* 407, 57 (2000).
- [3] B. Xu, N.J. Tao, Science **301**, 1221 (2003).
- [4] M.T. González, S. Wu, R. Huber, S.J. Van Der Molen, C. Schönenberger, M. Calame, Nano Lett. 6, 2238 (2006).
- [5] Z. Huang, B. Xu, Y. Chen, M.D. Ventra, N. Tao, *Nano Lett.* 6, 1240 (2006).
- [6] J. Reichert, R. Ochs, D. Beckmann, H. Weber, M. Mayor, H. von Löhneysen, *Phys. Rev. Lett.* 88, 176804 (2002).

- [7] M. Kiguchi, O. Tal, S. Wohlthat, F. Pauly, M. Krieger, D. Djukic, J.C. Cuevas, J.M. van Ruitenbeek, *Phys. Rev. Lett.* 101, 046801 (2008).
- [8] A.A. Fouladi, *Chin. Phys. B* **26**, 47304 (2017).
- [9] L. Patrone, S. Palacin, J. Charlier, F. Armand, J.P. Bourgoin, H. Tang, S. Gauthier, Phys. Rev. Lett. 91, 096802 (2003).
- [10] B. Xu, X. Xiao, N.J. Tao, J. Am. Chem. Soc. 125, 16164 (2003).
- [11] S. Kaneko, T. Nakazumi, M. Kiguchi, *J. Phys. Chem. Lett.* 1, 3520 (2010).
- [12] H. Song, M.A. Reed, T. Lee, Adv. Mater.23, 1583 (2011).
- [13] C. Joachim, J.K. Gimzewski, A. Aviram, *Nature* **408**, 541 (2000).
- [14] R.P. Andres, T. Bein, M. Dorogi, S. Feng, J.I. Henderson, C.P. Kubiak, W. Mahoney, R.G. Osifchin, R. Reifenberger, *Science* 272, 1323 (1996).
- [15] A. Aviram, M.A. Ratner, *Chem. Phys. Lett.* **29**, 277 (1974).
- [16] J.-X. Yu, X.-R. Chen, S. Sanvito, Y. Cheng, *Appl. Phys. Lett.* **100**, 013113 (2012).
- [17] C. Zhang, R.N. Barnett, U. Landman, *Phys. Rev. Lett.* **100**, 046801 (2008).
- [18] Y. Qi, D. Guan, Y. Jiang, Y. Zheng, C. Liu, Phys. Rev. Lett. 97, 256101 (2006).
- [19] S. Csonka, A. Halbritter, G. Mihály, O.I. Shklyarevskii, S. Speller, H. van Kempen, *Phys. Rev. Lett.* 93, 016802 (2004).
- [20] R.H.M. Smit, Y. Noat, C. Untiedt, N.D. Lang, M.C. van Hemert, J.M. van Ruitenbeek, *Nature* 419, 906 (2002).
- [21] W. Thijssen, D. Marjenburgh, R. Bremmer, J. Van Ruitenbeek, *Phys. Rev. Lett.* 96, 026806 (2006).
- [22] M. Strange, K.S. Thygesen, K.W. Jacobsen, *Phys. Rev. B* 73, 125424 (2006).
- [23] F.-T. Liu, Y. Cheng, F.-B. Yang, X.-R. Chen, *Chin. Phys. Lett.* **30**, 107303 (2013).
- [24] F.-T. Liu, Y. Cheng, F.-B. Yang, X.-R. Chen, *Chem. Phys. Lett.* **590**, 160 (2013).
- [25] F.-T. Liu, Y. Cheng, X.-R. Chen, X.-H. Cheng, *Acta Phys. Sin.* **63**, 137303 (2014).
- [26] F.-T. Liu, Y. Cheng, X.-H. Cheng, F.-B. Yang, X.-R. Chen, *Chin. Phys. Lett.* 30, 067302 (2013).
- [27] C.-Z. Gu, Q. Wang, J.-J. Li, K. Xia, *Chin. Phys. B* **22**, 098107 (2013).

- [28] A. Sedky, E. El-Suheel, Chin. Phys. B 21, 116103 (2012).
- [29] L. Li, C. Li, Y. Chen, *Physica E* **40**, 2513-2516 (2008).
- [30] Y.J. Chen, B. Chi, D.C. Mahon, Y. Chen, Nanotechnology 17, 2942 (2006).
- [31] O. Cretu, H.P. Komsa, O. Lehtinen, G. Algara-Siller, U. Kaiser, K. Suenaga, A.V. Krasheninnikov, ACS Nano 8, 11950 (2014).
- [32] Y. Rong, J.H. Warner, ACS Nano 8, 11907 (2014).
- [33] S. Zhang, Q. Wang, Y. Kawazoe, P. Jena, J. Am. Chem. Soc. 135, 18216 (2013).
- [34] S.-L. Wang, C.-L. Yang, M. Wang, X.G. Ma, J. Ludong Univ. 33, 26 (2017).
- [35] S.-L. Wang, C.-L. Yang, M. Wang, X.G. Ma, J.-G. Xin, Phys. Lett. A 381, 1493 (2017).
- [36] J. Zeng, K.-Q. Chen, Y.-X. Deng, *Physica E* 114, 113565 (2019).
- [37] M. Brandbyge, J.L. Mozos, P. Ordejón, J. Taylor, K. Stokbro, *Phys. Rev. B* 65, 165401 (2002).
- [38] W. Kohn, L.J. Sham, *Phys. Rev.* **140**, A1133 (1965).
- [39] A.-P. Jauho, N.S. Wingreen, Y. Meir, *Phys. Rev. B* **50**, 5528 (1994).
- [40] J. Taylor, H. Guo, J. Wang, Phys. Rev. B 63, 245407 (2001).
- [41] C. Caroli, R. Combescot, P. Nozieres, D. Saint-James, J. Phys. C Solid State Phys. 4, 916 (1971).
- [42] L.V. Keldysh, Sov. Phys. JETP **20**, 1018 (1965).
- [43] S. Datta, Electronic Transport in Mesoscopic Systems, Cambridge University Press, Cambridge 1995.
- [44] M. Büttiker, Y. Imry, R. Landauer, S. Pinhas, *Phys. Rev. B* 31, 6207 (1985).
- [45] J.P. Perdew, A. Zunger, *Phys. Rev. B* **23**, 5048 (1981).
- [46] N. Troullier, J.L. Martins, Phys. Rev. B 43, 1993 (1991).
- [47] L. Kleinman, D.M. Bylander, *Phys. Rev. Lett.* 48, 1425 (1982).
- [48] T. Zhang, Y. Cheng, X.-R. Chen, RSC Adv. 4, 51838 (2014).
- [49] D. Çakır, O. Gülseren, Phys. Rev. B 84, 085450 (2011).
- [50] P.N. D'yachkov, V.A. Zaluev, S.N. Piskunov, Y.F. Zhukovskii, RSC Adv. 5, 91751 (2015).
- [51] R.T. Senger, S. Tongay, E. Durgun, S. Ciraci, Phys. Rev. B 72, 75419 (2005).

- [52] A. Abdurahman, A. Shukla, M. Dolg, Phys. Rev. B 65, 115106 (2002).
- [53] I.S. Kristensen, D.J. Mowbray, K.S. Thygesen, K.W. Jacobsen, J. Phys. Condens. Matter 20, 374101 (2008).
- [54] J.-X. Yu, Y. Cheng, S. Sanvito, X.-R. Chen, *Appl. Phys. Lett.* **100**, 103110 (2012).
- [55] I.I. Oleynik, M.A. Kozhushner, V.S. Posvyanskii, L. Yu, *Phys. Rev. Lett.* **96**, 096803 (2006).
- [56] Y. Mu, Z.-Y. Zeng, Y. Cheng, X.-R. Chen, $RSC\ Adv.\ \mathbf{6},\ 91453\ (2016)$.
- [57] H. Weber, J. Reichert, R. Ochs, D. Beckmann, M. Mayor, H. Löhneysen, *Physica E* 18, 231 (2003).
- [58] J.B. Pan, Z.H. Zhang, K.H. Ding, X.Q. Deng, C. Guo, Appl. Phys. Lett. 98, 092102 (2011).